

Pd/B₄C/Y multilayer coatings for extreme ultraviolet applications near 10 nm wavelength

DAVID L. WINDT^{1,*} AND ERIC M. GULLIKSON²

¹Reflective X-ray Optics LLC, 1361 Amsterdam Ave, New York, New York 10027, USA

²Lawrence Berkeley National Laboratory, 1 Cyclotron Road, Berkeley, California 94270, USA

*Corresponding author: davidwindt@gmail.com

Received 31 March 2015; revised 20 May 2015; accepted 21 May 2015; posted 29 May 2015 (Doc. ID 237303); published 19 June 2015

A new extreme ultraviolet (EUV) multilayer coating has been developed comprising Pd and Y layers with thin B₄C barrier layers at each interface, for normal incidence applications near 10 nm wavelength. Periodic, nonperiodic, and dual-stack coatings have been investigated and compared with similar structures comprising either Mo/Y or Pd/B₄C bilayers. We find that Pd/B₄C/Y multilayers provide higher reflectance than either Mo/Y or Pd/B₄C, with much lower film stress than Pd/B₄C. We have also investigated the performance of periodic multilayers comprising repetitions of Pd/Y, Ru/Y, or Ru/B₄C/Y, as well as Pd/B₄C multilayers deposited using reactive sputtering with an Ar:N₂ gas mixture in order to reduce stress: these material combinations were all found to provide poor EUV performance. The temporal stability of a periodic Pd/B₄C/Y multilayer stored in air was investigated over a period of 16 months, and a slight reduction in peak reflectance was observed. Periodic Pd/B₄C/Y multilayers were also found to be thermally stable up to 100°C; at higher temperatures (200°C and 300°C) we observe a slight reduction in peak reflectance and a slight increase in multilayer period. High-resolution transmission electron microscopy and selected area diffraction of an as-deposited Pd/B₄C/Y film indicates a fully amorphous structure, with interfaces that are both smoother and more abrupt than those observed in a comparable Pd/B₄C multilayer in which the Pd layers are polycrystalline. The new Pd/B₄C/Y multilayers are suitable for normal-incidence imaging and spectroscopy applications, including solar physics, plasma physics, high-brightness EUV light sources, and others. © 2015 Optical Society of America

OCIS codes: (230.4170) Multilayers; (310.4165) Multilayer design; (340.7470) X-ray mirrors; (340.7480) X-rays, soft x-rays, extreme ultraviolet (EUV).

<http://dx.doi.org/10.1364/AO.54.005850>

1. INTRODUCTION

Nanometer-scale multilayer films developed in recent years have enabled the production of optical elements such as mirrors and gratings that operate near normal incidence in the extreme ultraviolet (EUV) wavelength range. Normal-incidence, multilayer-coated optics have in turn been used in the construction of a variety of instruments for applications including solar physics, plasma physics, high-brightness light sources, photolithography, and others.

The multilayer coating having the best EUV performance demonstrated thus far is Si/Mo [1], which can now provide peak reflectance near 70%. The high reflectance achievable with Si/Mo spawned the EUV lithography industry, and has been used in the construction of a number of important satellite instruments for solar physics over the past three decades as well. However, Si/Mo has relatively low reflectance at wavelengths shorter than 12.4 nm wavelength (i.e., the Si L-edge), due to high optical absorption in the Si layers. Consequently, a

variety of other multilayer material combinations have been investigated over the years for use at these shorter wavelengths [2–6].

The wavelength range from $\lambda \sim 9\text{--}14$ nm is of particular interest for solar physics, due to the bright coronal Fe XVIII line at $\lambda = 9.4$ nm, the bright lines of Fe VIII, XX, and XXIII near $\lambda = 13.1$ nm, and other weaker emission lines as well [7]. The AIA instrument onboard the Solar Dynamics Observatory [8] and the SUVI instrument [9] on the GOES-R satellite currently scheduled for launch in 2016 both have dedicated imaging channels tuned to these two wavelengths, using periodic Si/Mo multilayer coatings for the 13.1 nm channel, and Mo/Y multilayer coatings for the 9.4 nm channel. Mo/Y multilayer films provide relatively high peak reflectance ($R_{\max} \sim 0.33$) at $\lambda = 9.4$ nm, have very low stress, and have been demonstrated to be stable over time.

Future EUV imaging instruments for solar physics having higher spatial and temporal resolution, however, will require narrowband reflectance that is higher than is achievable with

Mo/Y at $\lambda = 9.4$ nm, in order to support the signal-to-noise and exposure times needed to capture the evolution of dynamic processes in the solar atmosphere [10]. Furthermore, high-resolution spectroscopy instruments using multilayer-coated diffraction gratings operating near normal incidence and targeting the $\lambda \sim 9\text{--}14$ nm band [11] will require nonperiodic multilayer coatings having a broad spectral response, constructed from materials other than Si in order to achieve good performance at wavelengths shorter than the Si L-edge.

The primary objectives of the research described here are thus to develop new normal-incidence multilayer coatings that provide (a) higher reflectance than Mo/Y, for narrowband solar imaging near 9.4 nm and (b) high reflectance over a broad spectral band in the $\lambda \sim 9\text{--}14$ nm wavelength range, for high-resolution spectroscopy. The new multilayer coatings must also have relatively low film stress, in order to avoid any stress-induced adhesion failures or other, related problems.

Periodic, narrowband Pd/B₄C multilayers have been shown recently [3] to have significantly higher peak reflectance than Mo/Y near 9 nm wavelength. However, the films developed thus far also have extremely high stress. Ru/B₄C multilayers have been demonstrated to have relatively high reflectance as well at wavelengths longer than the B-K edge near 6.7 nm [12], but also suffer from unacceptably high film stress.

Motivated by the good EUV performance achieved with Mo/Y, Pd/B₄C, and Ru/B₄C, we have investigated several new multilayer material combinations: Pd/Y, Ru/Y, Pd/Y with thin B₄C barrier layers at each interface to mitigate diffusion, and Ru/Y with B₄C barrier layers. We have also investigated the growth of Pd/B₄C multilayers using reactive sputtering with an Ar-N₂ gas mixture in place of pure Ar, a technique that we have found in the past to effectively reduce film stress in a number of other multilayer material combinations [13,14]. As explained below in detail, we find the best results with Pd/Y multilayers having B₄C barrier layers. We have thus designed, fabricated, and tested a number of periodic and nonperiodic Pd/B₄C/Y multilayers, and compared their EUV reflectance and film stress with similar coatings comprising repetitions of Pd/B₄C or Mo/Y. We have also studied the temporal and thermal stability of Pd/B₄C/Y multilayers, and have compared layer microstructure and interface properties of periodic Pd/B₄C and Pd/B₄C/Y multilayers using high-resolution transmission electron microscopy and selected area electron diffraction.

We describe in Section 2 the experimental techniques used for the growth and characterization of these new multilayer coatings, and we present our experimental results in Section 3. We conclude in Section 4 with a summary of our findings, a discussion of their implications for the development of future EUV instrumentation, and prospects for further multilayer research.

2. EXPERIMENTAL

Multilayer films were deposited by magnetron sputtering, using the deposition system shown schematically in Fig. 1. The system uses three circular “S-gun” magnetron sources, with two-piece cylindrical targets, the largest measuring 4.7 cm in diameter. The magnetron sources are mounted in the bottom flange of the vacuum chamber and face up. Shaped metal

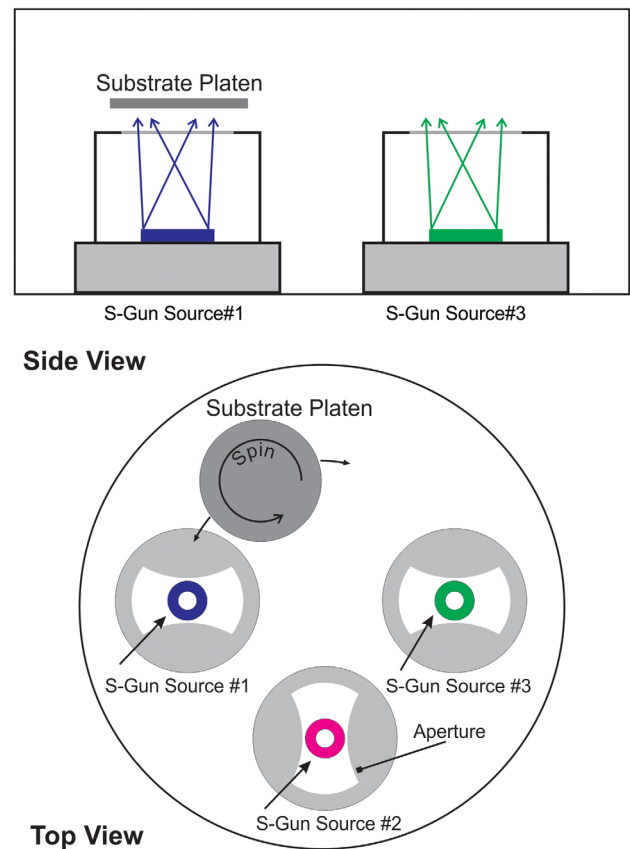


Fig. 1. Schematic diagram of the magnetron deposition system used for multilayer deposition. The system uses three circular “S-Gun” magnetron sources and a planetary substrate motion.

apertures are located 95 mm above each source to improve coating uniformity. The substrate faces down, and a stepper-motor-driven planetary mechanism is used to rotate the substrate past each magnetron source, building up a multilayer film one layer at a time; the substrate also spins at ~ 100 rpm as it rotates, also to improve coating uniformity. The target-to-substrate distance is fixed at 110 mm. The deposited film thickness is proportional to the amount of time that the substrate is exposed to the magnetron source, and thus is inversely proportional to the specified substrate rotational velocity. Thus, by controlling the substrate rotational velocity in real time as it passes over each magnetron source, arbitrary layer thicknesses can be deposited. No deposition shutters are used in this system.

Films were deposited onto polished Si (100) wafer substrates measuring 75 mm in diameter. The substrates were unheated and ungrounded during film deposition. Target purities were 99.95% for Pd, 99.9% for Ru, 99.9% for Y, 99.95% for Mo, and 99.95% for B₄C. Either Pd, Ru, or Mo were used for the top-most layer in all films described here. DC power supplies were used in constant-power mode for all materials, with Pd, Ru, and Mo operated at 40 W, and Y and B₄C at 60 W. The working gas was Ar of 99.999% purity, or, in the case of reactively sputtered films, various mixtures of Ar and N₂ (99.999% purity), with the working gas pressure held at

1.9 mTorr in all cases using a closed-loop gas flow system comprising mass-flow controllers and a capacitance manometer. The deposition system uses both a turbo pump and a cryo-pump; all films were deposited after several hours of pumping, when the background pressure fell below 2×10^{-7} Torr.

Structural analysis of deposited films was investigated with grazing-incidence x-ray reflectometry (XRR), using an x-ray diffractometer system operating in the θ - 2θ mode. The system is constructed from a sealed-tube x-ray source having a Cu anode, a flat Ge monochromator crystal adjusted to select the Cu K- α line complex near $\lambda = 1.542$ Å, a 4-circle high-resolution goniometer, a Si:Li x-ray detector, and pulse counting electronics. X-ray reflectance curves were analyzed using IMD [15]: specifically, layer thicknesses were derived by modeling the measured XRR data.

Film stress was measured using the wafer-curvature technique, with a commercial dual-wavelength laser-scanning system (Toho Technologies, Flexus Model 2323-S). Wafer curvature was measured before and after film deposition, and using the measured film thickness and the known properties of the Si (100) substrates, film stress was computed from the Stoney equation. The system can be used to measure film stress for as-deposited coatings, as well as for measurements of stress as a function of temperature as the sample is heated and cooled.

Normal-incidence reflectance measurements were made with an EUV reflectometer [16], located at Reflective X-ray Optics (RXO), comprising a laser-produced plasma source, a grating monochromator, a custom vacuum goniometer having six degrees of freedom, a Si avalanche photodiode (APD) detector, and detector electronics that include a pre-amp, a pulse-shaping amplifier, and a gated integrated/boxcar averager. A frequency-doubled Nd:YAG laser provides ~ 10 ns pulses having ~ 500 mJ of energy at $\lambda = 532$ nm, at a repetition rate of 10 Hz. The laser beam is focused (through a fused-silica vacuum window) to a diameter of ~ 100 μm , using a simple plano-convex lens, onto a solid Cu target in order to generate a highly ionized Cu plasma that effectively provides continuum EUV radiation. The monochromator is used for wavelength selection, and comprises fixed entrance and exit slits (set for this work to 50 and 100 μm widths, respectively), and an adjustable, gold-coated, varied-line-space diffraction grating. The incidence angle on the grating, which determines the wavelength of light passing through the exit slit and reaching the sample under test, is adjusted by a mechanism that uses a stepper-motor-driven rotary feed-through. The monochromator also uses gold-coated spherical mirrors operating at 2° grazing incidence to (astigmatically) collimate the beam in both directions. In addition, for the measurements described here, four Ru-coated flat mirrors, operating at 8° grazing incidence and arranged in series along the beam path in order to exploit the effect of total external reflection, were used to suppress higher orders that are diffracted from the grating and that also pass through the exit slit; i.e., wavelengths shorter than $\lambda \sim 7$ nm are effectively suppressed by the Ru mirror system. Horizontal and vertical slits are used to adjust the final size of the collimated pencil beam on the sample to 1 mm wide \times 2 mm high. A microchannel-plate detector (with detector

electronics equivalent to those used for the avalanche photodiode detector described above) is used to sample the intensity of the incident beam before it reaches these slits, so that shot-to-shot intensity fluctuations intrinsic to the light source can be removed from the primary signal produced by the APD detector. The goniometer is used to position the APD detector and the mirror under test relative to the incidence beam. With the mirror positioned out of the beam, the spectrum of the incident beam is first measured (i.e., intensity as a function wavelength, determined by measuring intensity as the grating angle is varied in discrete steps); the spectrum of the beam reflected by the mirror at the desired incidence angle (5° for this work) is then measured, and the reflectance is computed as the reflected spectrum divided by the incident spectrum.

In addition to EUV reflectance measurements made using the laser-plasma-source reflectometer at RXO, selected samples were measured using synchrotron radiation at the advanced light source (ALS) calibration and standards beam line 6.3.2. The ALS reflectometer [17] has much higher signal-to-noise, dynamic range, spectral resolution, and spectral purity than the RXO reflectometer, and thus produces more precise and accurate measurements. We find that reflectance measurements of periodic multilayers, for example, made at the ALS show systematically higher peak reflectance values than we measure using the RXO reflectometer, due to the latter system's reduced spectral resolution and spectral purity. To illustrate, shown in Fig. 2 are reflectance-versus-wavelength measurements, made at both the ALS and at RXO, of two different periodic Mo/Y multilayers. In spite of the systematic errors intrinsic to the RXO reflectometer that result in reduced peak reflectance and degraded resolution of fine structure, that system is nevertheless useful for, e.g., rapid feedback during multilayer development.

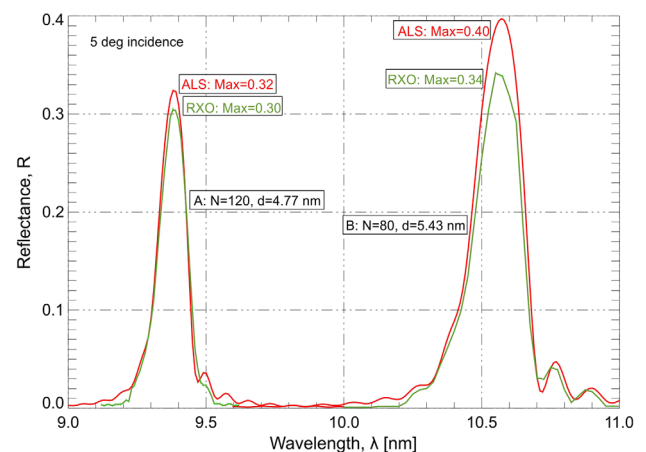


Fig. 2. EUV reflectance of two Mo/Y periodic multilayer films, comparing measurements obtained using either synchrotron radiation at the ALS, or using a laser-produced plasma-source reflectometer at RXO, as labeled. Sample A has $N = 120$ repetitions and a period of $d = 4.77$ nm; sample B has $N = 80$ and $d = 5.43$ nm. The RXO reflectometer yields peak reflectance values that are systematically low relative to the ALS reflectometer, due to reduced spectral resolution and spectral purity.

3. RESULTS

A. Periodic Multilayers

In an effort to reduce the high film stress found in Pd/B₄C coatings, a series of periodic multilayers was fabricated by reactive sputtering using an Ar:N₂ gas mixture that ranged in composition from 0% to 22% N₂ by volume. Periodic multilayer films are characterized by the period, d , equal to the thickness of one repetition, and the number of repetitions, N . For the Pd/B₄C films studied here, each film contained $N = 120$ repetitions and had a multilayer period in the range $d = 4.4\text{--}4.5$ nm.

Reactive sputtering was indeed effective at reducing film stress: the film deposited with pure Ar had stress of -1200 MPa (compressive), while the films deposited by reactive sputtering with Ar:N₂ mixtures all had stresses below $+60$ MPa (tensile). However, as illustrated in Fig. 3, the EUV reflectance of the reactively sputtered films was found to be poor in all cases.

We next investigated periodic multilayers comprising material combinations of Pd/Y and Ru/Y, both with and without 0.7-nm-thick B₄C barrier layers deposited at each interface to mitigate diffusion of material across the interface. The films had periods in the range $d = 4.35$ to 4.85 nm. XRR, EUV reflectance, and film stress measurements were made in each case, with the exception of the Pd/Y film deposited with no barrier layers: the first-order Bragg peak is strongly suppressed in the XRR measurements shown in Fig. 4 for a test film comprising only $N = 20$ repetitions of Pd/Y, suggesting significant interface diffusion in this film, which in turn suggests low EUV reflectance; consequently, we abandoned the plan to experimentally investigate the EUV performance and stress in a Pd/Y film having $N = 100$ repetitions (i.e., the number of repetitions needed for high reflectance). Shown in Fig. 5, however, are the XRR, EUV, and film stress results for Pd/B₄C/Y, Ru/Y, and Ru/B₄C/Y multilayers, each having $N = 100$ repetitions. Measured film stresses are below -400 MPa

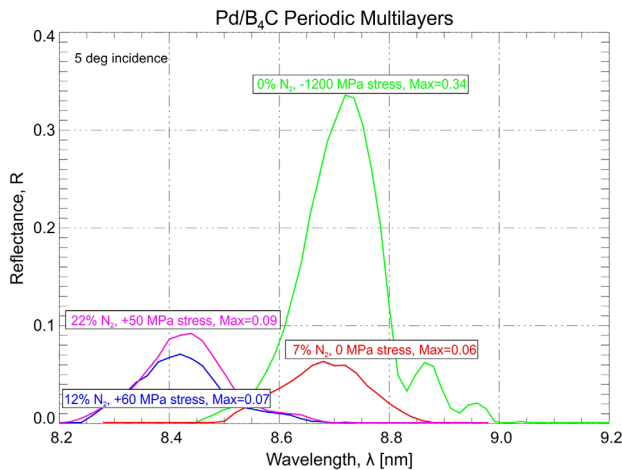


Fig. 3. Measured EUV reflectance of Pd/B₄C multilayers deposited by reactive sputtering using an Ar/N₂ gas mixture, relative to a Pd/B₄C multilayer deposited by nonreactive sputtering using only Ar gas. N₂ concentration, film stress, and peak reflectance values are labeled. Reactive sputtering reduces film stress significantly, but the EUV reflectance is poor.

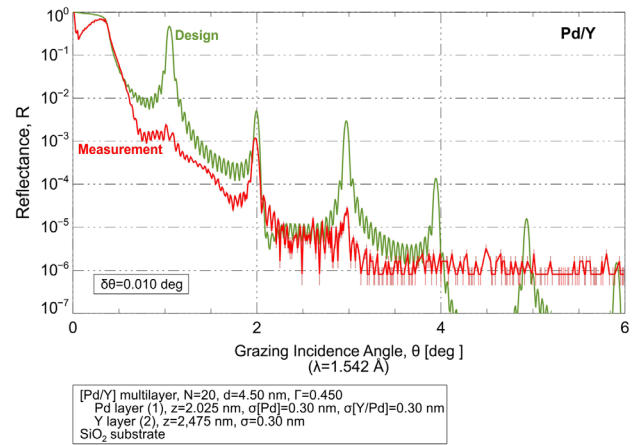


Fig. 4. XRR results of a Pd/Y multilayer having $N = 20$ repetitions, and a period of $d = 4.5$ nm. While the second- and third-order Bragg peaks, near $\theta = 2^\circ$ and $\theta = 3^\circ$, respectively, are well defined in the measured data, the first-order Bragg peak expected near $\theta = 1^\circ$ is strongly suppressed. This is likely due to interface diffusion, and would suggest low EUV reflectance.

(compressive) in all three cases. The XRR results for all three films show strong first-order Bragg peaks, and good agreement with IMD calculations made assuming interface widths of $\sigma = 0.3$ nm. In spite of the good XRR performance, however, the Ru/Y and Ru/B₄C/Y films have relatively poor EUV reflectance. In contrast, the Pd/B₄C/Y multilayer has relatively high reflectance, $R_{\max} = 0.38$ near $\lambda = 9.4$ nm, as measured with the RXO reflectometer. The IMD simulations of EUV reflectance shown in Fig. 5 were made using the layer thicknesses determined from the XRR data, but with interface widths of $\sigma = 0.85$ nm for Pd/B₄C/Y, $\sigma = 0.835$ nm for Ru/Y, and $\sigma = 0.75$ nm for Ru/B₄C/Y; these interface width values produce peak reflectance values approximately equal to the measured peak reflectance values in all three cases. However, in spite of the agreement in peak reflectance obtained using these parameter values, the shapes of the models differ from the measurements in all cases, with the largest disparities observed in the case of the two Ru-based multilayers. Such disparities might be due to errors in the *relative* layer thicknesses derived from XRR modeling, to different interface properties than those assumed in the models, to surface oxides not included in the IMD models, or to inaccuracies in the optical constants in the 8–10 nm band for these materials.

B. B₄C Barrier Layer Thickness Optimization

In light of the good EUV results and relatively low stress obtained with the periodic Pd/B₄C/Y multilayer film shown in Fig. 5, we subsequently deposited a series of periodic Pd/B₄C/Y multilayers, all having $d \sim 4.9$ nm and $N = 100$, for which we systematically varied the B₄C thickness from 0.5 to 0.8 nm, in 0.1 nm steps, in order to identify the optimal B₄C barrier layer thickness. The peak reflectance near normal incidence varied only slightly (as measured at RXO) over this range of barrier layer thicknesses, from $R_{\max} = 0.38$ to 0.40; barrier layer thicknesses of $d_{\text{B}_4\text{C}} = 0.6$ nm were nevertheless found to yield the highest peak reflectance. The as-deposited stresses

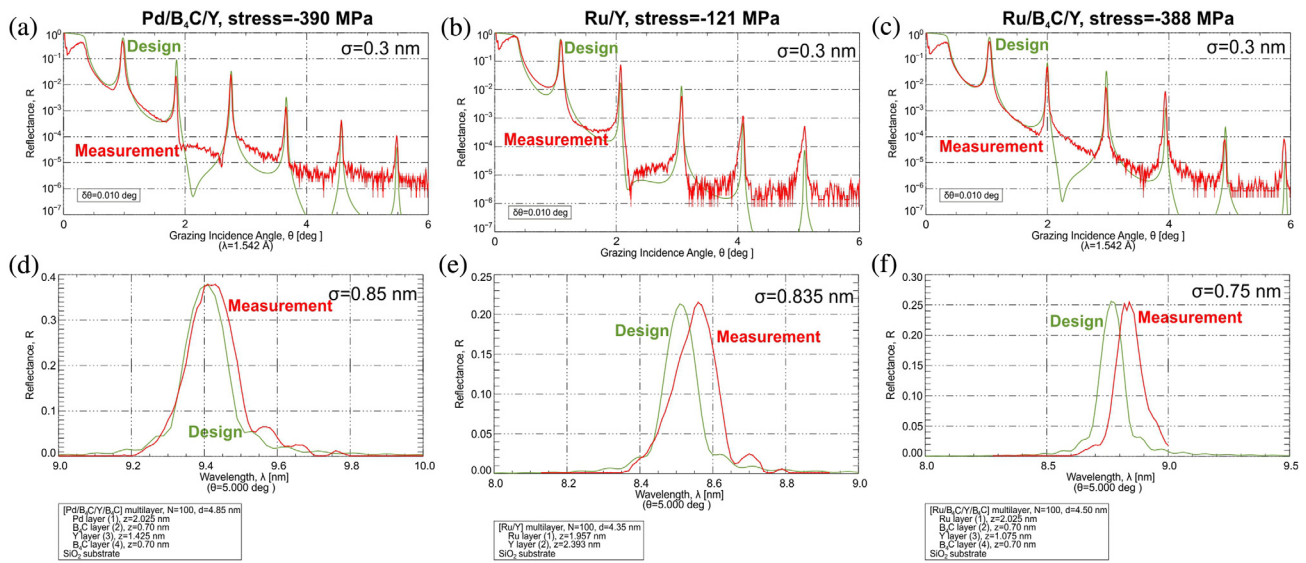


Fig. 5. XRR (top row) and EUV (bottom row) results for (a) Pd/B₄C/Y, (b) Ru/Y, and (c) Ru/B₄C/Y multilayers, each having $N = 100$ repetitions. 0.6-nm-thick B₄C barrier layers were used for both the Pd/B₄C/Y and Ru/B₄C/Y multilayers. Measured film stresses are indicated, as are the interface widths σ used for the IMD calculations, which are also shown. The multilayer periods determined from XRR measurements were used for the calculations of EUV reflectance.

of these films were found to increase monotonically from -400 MPa for $d_{B_4C} = 0.5$ nm to -567 MPa for $d_{B_4C} = 0.8$ nm. In light of these results, subsequent films were made with $d_{B_4C} = 0.6$ nm.

Shown in Fig. 6 are the normal-incidence reflectance curves measured at the ALS for periodic multilayers tuned near 9.4 nm comprising repetitions of Mo/Y, Pd/B₄C, or Pd/B₄C/Y with 0.6-nm-thick B₄C barrier layers at each interface. The as-deposited film stresses and peak reflectance values are labeled. The Pd/B₄C/Y multilayer provides the highest peak reflectance ($R_{\max} = 0.43$), and acceptably low film stress (-480 MPa).

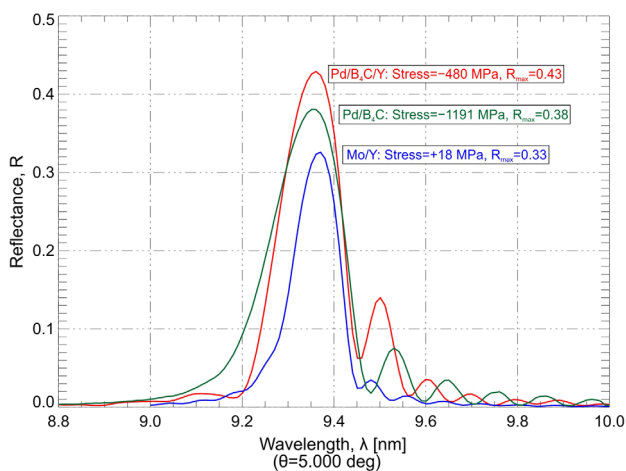


Fig. 6. EUV reflectance measured at 5° incidence at the ALS for periodic multilayer coatings comprising repetitions of Mo/Y, Pd/B₄C, or Pd/B₄C/Y/B₄C, as indicated. As-deposited film stresses and peak reflectance values are labeled.

C. Nonperiodic Multilayers

A variety of nonperiodic multilayer films having broad spectral response were designed using IMD. Such coatings would be needed for high-resolution spectroscopy using multilayer-coated gratings operating at normal incidence. The nonperiodic coatings were fabricated and tested, and were compared with similar coating designs using Pd/B₄C bilayers. In addition, three different nonperiodic multilayers comprising Mo/Y bilayers were investigated as well. For each of the three material combinations, both depth-graded and aperiodic designs were explored. Two of the Mo/Y films were designed for broad spectral response from 9 to 14 nm wavelength, while the third Mo/Y film, and all four Pd/B₄C and Pd/B₄C/Y films, were designed for high reflectance in the 8.9 to 11.2 nm wavelength band.

The first Mo/Y design contains $N = 120$ repetitions and uses an analytic distribution of layer thicknesses with depth in the film, as illustrated in Fig. 7(a): the Y layer thicknesses range from 2 to 4.0425 nm, and the thickness of each Y layer is given by $d_Y(j) = 4.0425 - 4.266 \times \ln(j)$ nm, where j is the layer index, as measured from the top of the film. The Mo layer thickness in each Mo/Y bilayer is given by $d_{Mo}(j) = 0.81782 \times d_Y(j)$, with d_{Mo} thus ranging from 1.6356 to 3.306 nm. We also investigated Pd/B₄C and Pd/B₄C/Y films following a similar so-called “ln-graded” design, each containing $N = 80$ repetitions. For the Pd/B₄C film [Fig. 7(b)], the Pd and B₄C layer thicknesses are equal in each bilayer, and both range in thickness from 2 to 3.1 nm. The distribution of Pd and B₄C layer thicknesses with depth in the film is described by $d_{Pd}(j) = d_{B_4C}(j) = 3.1 - 2.51 \times \ln(j)$ nm. In the case of the Pd/B₄C/Y film that follows this same design [Fig. 7(c)], the Pd layer thicknesses have the same analytic distribution, but each B₄C layer in the Pd/B₄C design is replaced by a B₄C/Y/B₄C trilayer of the same thickness, with both B₄C

layer thicknesses fixed at 0.6 nm for all repetitions. Thus the Y layer thicknesses are given by $d_Y(j) = 3.1 - 2.51 \times \ln(j) - 2 \times d_{B_4C} = 1.9 - 2.51 \times \ln(j)$ nm.

In the second type of nonperiodic coating design, a genetic algorithm was used in IMD to design fully aperiodic structures [18] (i.e., with numerical, rather than analytic, layer thickness

distributions) having a nominally flat response at 5° incidence: from 9 to 14 nm wavelength for one of the aperiodic Mo/Y films [Fig. 7(d)], and from 8.9 to 11.2 nm wavelength for the third nonperiodic Mo/Y film [Fig. 7(e)], and for both Pd/B₄C [Fig. 7(f)] and Pd/B₄C/Y [Fig. 7(g)] films as well. In the case of the first Mo/Y aperiodic film designed for the

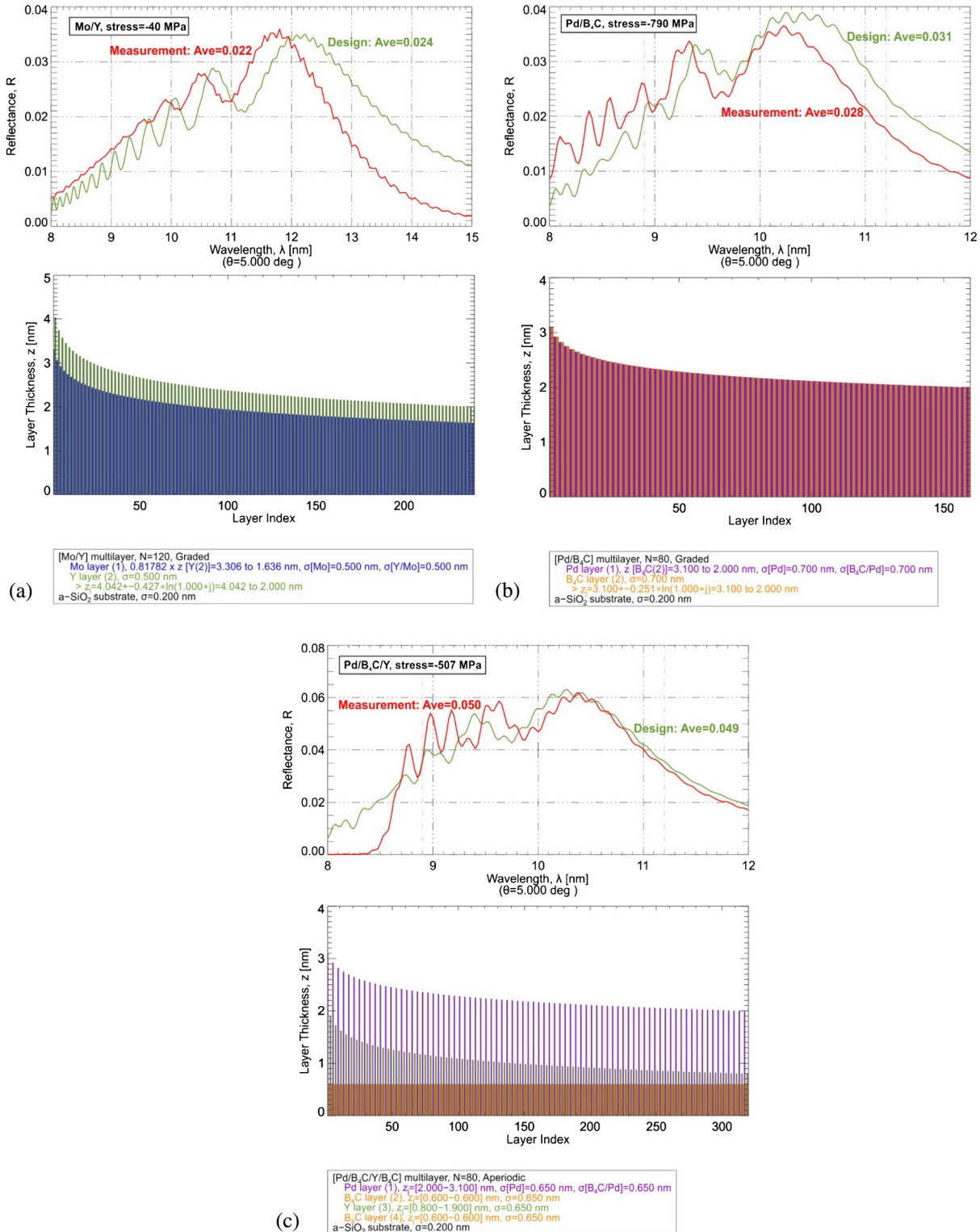


Fig. 7. (Continued)

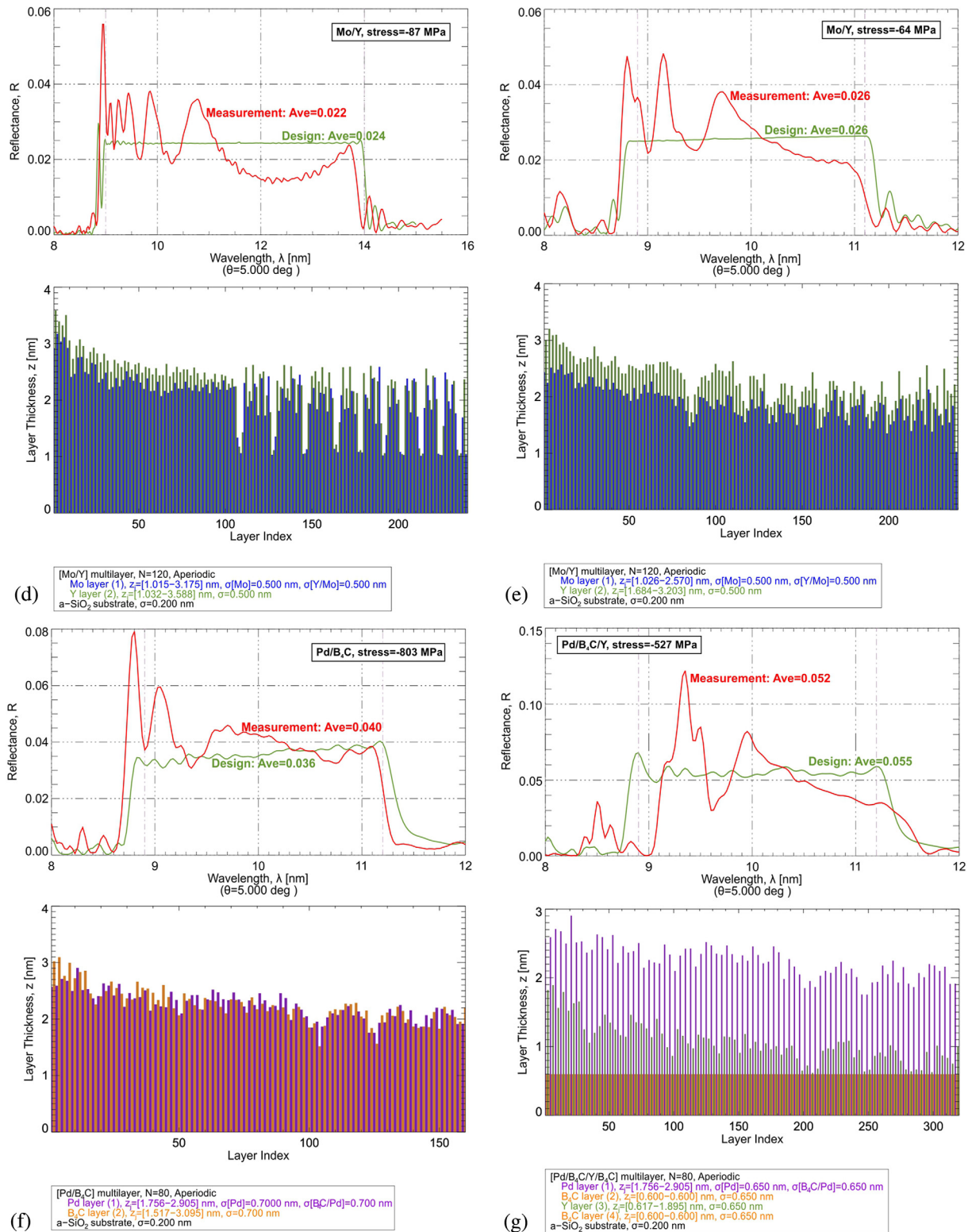


Fig. 7. EUV reflectance measured at 5° incidence at the ALS, and modeled using IMD (top), and layer thickness distribution (bottom), for nonperiodic multilayers: “In-graded” analytic designs with repetitions of (a) Mo/Y, (b) Pd/B₄C, and (c) Pd/B₄C/Y/B₄C; (d) an aperiodic Mo/Y multilayer designed for flat response from 8.9 to 1.4 nm wavelength; and aperiodic multilayers designed for flat response from 8.9 to 1.12 nm comprising repetitions of (e) Mo/Y, (f) Pd/B₄C, and (g) Pd/B₄C/Y/B₄C. Average reflectance values are labeled, and were computed, using the interface widths σ indicated in the legends, from 8.9 to 1.4 nm for (a) and (d), and from 8.9 to 1.12 nm for (b), (c), and (e) through (g).

9 to 14 nm range, the Mo thicknesses ranged from $d_{\text{Mo}} = 1.0149$ to 3.1754 nm, the Y thicknesses ranged from $d_{\text{Y}} = 1.0319$ to 3.588 nm, and $N = 120$ repetitions were used. In the second Mo/Y aperiodic film, designed for the 8.9 to 11.2 nm range, the Mo thicknesses ranged from $d_{\text{Mo}} = 1.0255$ to 2.5703 nm, and the Y thicknesses ranged from $d_{\text{Y}} = 1.6824$ to 3.2033 nm, also with $N = 120$ repetitions. For the Pd/B₄C film, which contained $N = 80$ repetitions, the Pd layer thicknesses ranged from $d_{\text{Pd}} = 1.756$ to 2.9048 nm and the B₄C layer thicknesses ranged from $d_{\text{B}_4\text{C}} = 1.5174$ to 3.0945 nm. For the Pd/B₄C/Y film, the same number of repetitions was used, and the B₄C layer thicknesses were again fixed at 0.6 nm, while the Pd thicknesses varied from $d_{\text{Pd}} = 1.756$ to 2.9048 nm, and the Y thicknesses varied from $d_{\text{Y}} = 0.6174$ to 1.8945 nm.

After deriving deposition rates for Mo, Y, Pd, and B₄C, using XRR measurements of test films to determine layer thicknesses along with the known rotational velocities used to deposit those test films, the seven different nonperiodic multilayer films just described were grown and tested. As-deposited film stress was measured using wafer-curvature, as described above, and EUV reflectance measurements were made at 5° incidence at the ALS. The results are shown in Fig. 7, along with the plots of the nominal layer thickness distributions referred to above. The measured stresses are labeled. The nominal EUV response curves computed using IMD are shown as well. For these computations, interface widths of $\sigma = 0.65$ nm were used for Pd/B₄C/Y, $\sigma = 0.70$ nm for Pd/B₄C, and $\sigma = 0.50$ for Mo/Y.

As can be seen in Fig. 7, significant disparities between the measured and calculated EUV reflectance curves are evident in each case, and are largest for the Pd/B₄C/Y films. As discussed above, such disparities can be due to (i) inaccuracies in the optical constants of these materials (as is already suspected from the data for periodic films shown in Fig. 3), (ii) different interface properties than those assumed in the models, (iii) surface oxides, or (iv) layer thickness errors. Significant layer thickness errors can easily manifest as a result of inaccuracies in the derived deposition rates for each material, and could be the dominant source of error in the films shown in Fig. 7. Deposition rate inaccuracies stem from limitations on XRR modeling of the measured response used to derive individual layer thicknesses (particularly challenging in the case of three-material systems like Pd/B₄C/Y), and from the finite run-to-run repeatability of the deposition system, which is estimated to be relatively large for these materials, $\pm 1\%$ at best. Furthermore, the aperiodic designs are more sensitive to thickness errors than are the depth-graded designs, and the disparities between measurement and design are indeed largest for the aperiodic films. In any case, and in spite of the disparities between design and measurement evident in the films made thus far, we can see that the nonperiodic Pd/B₄C/Y films yield the highest reflectance over the 8.9 to 11.2 nm band, with the ln-graded design providing a relatively smooth response and an average reflectance of $R_{\text{ave}} = 0.05$ computed over this range. The Pd/B₄C/Y films also have significantly lower film stresses than the comparable Pd/B₄C films, e.g., -507 MPa for the ln-graded Pd/B₄C/Y film versus -790 MPa for the

ln-graded Pd/B₄C film. The Mo/Y films all have film stress well below 100 MPa, but also have the lowest reflectance.

D. Dual-Stack Multilayers

As an alternative to the broadband, nonperiodic coating designs discussed above, so-called “dual-stack” periodic multilayer coatings—comprising one periodic multilayer deposited on top of another—can be used to provide high reflectance in two wavelength bands [19]. For high-resolution spectroscopy of the solar corona, an instrument could be constructed using a grating coated with such a dual-stack multilayer that provides high normal-incidence reflectance, e.g., near the coronal Fe lines at $\lambda = 9.4$ nm and $\lambda = 13.1$ nm. Such a coating could also be used for solar imaging, in principle (provided that the reflectance is sufficiently high); for imaging of the Fe lines near $\lambda = 9.4$ nm and $\lambda = 13.1$ nm, the dual-stack coating could be used in conjunction with selectable Zr and Be transmission filters.

We have fabricated and tested two such dual-stack periodic multilayer coatings, one comprising Pd/B₄C bilayers, the other comprising Pd/Y bilayers with 0.6-nm-thick B₄C barrier layers. In both cases, the film designs contain a bottom periodic multilayer having $d = 4.75$ nm and $N = 30$, and a top periodic multilayer having $d = 6.9$ nm and $N = 8$. The normal-incidence reflectance curves for these coatings, as measured at the ALS, are shown in Fig. 8; the as-deposited stresses and peak reflectance values are indicated. As in the case of the periodic and nonperiodic films discussed above, the Pd/B₄C/Y dual-stack coating provides higher peak reflectance (in both wavelength bands) than Pd/B₄C, and also has significantly lower film stress: -469 MPa versus -1753 MPa for Pd/B₄C.

E. Temporal Stability of Pd/B₄C/Y

To assess the temporal stability of periodic Pd/B₄C/Y multilayer coatings, we have periodically remeasured the EUV reflectance (using the RXO reflectometer) of the film shown in Fig. 5 having B₄C barrier layers of thickness $d_{\text{B}_4\text{C}} = 0.7$ nm. The film was stored in air at room temperature since it was deposited. While the as-deposited peak reflectance (Fig. 5)

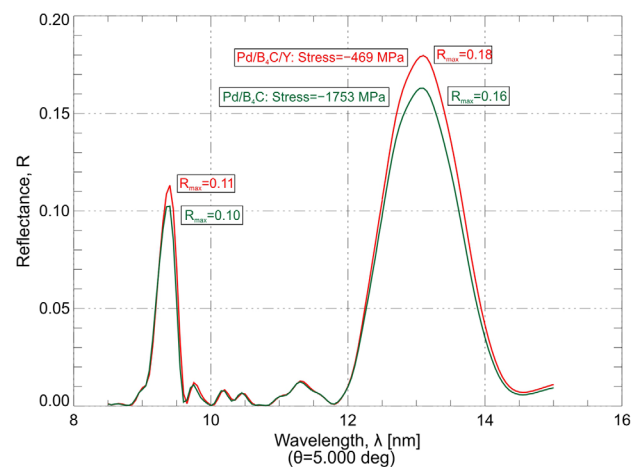


Fig. 8. EUV reflectance measured at 5° incidence at the ALS for dual-stack coatings comprising repetitions of either Pd/B₄C or Pd/B₄C/Y, as indicated. As-deposited film stresses and peak reflectance values are labeled.

was measured to be $R_{\max} = 0.38$, we found a steady decrease in peak reflectance over time: the peak reflectance dropped to $R_{\max} = 0.37$ after just a few days, and after 16 months we measured $R_{\max} = 0.34$. No wavelength shift was observed. XRR measurements of this film were also made periodically over 16 months, and the results are shown in Fig. 9. The Bragg peaks are essentially unchanged over time; however, the reflectance between the Bragg peaks has clearly evolved. The changes in XRR, as well as the drop in peak EUV reflectance observed over time, can be due to the growth of a Pd-oxide on the top surface of the film, or to chemical or structural changes at the interfaces.

F. Thermal Stability of Pd/B₄C/Y

The thermal stability of a periodic Pd/B₄C/Y multilayer having barrier layers of thickness $d_{B_4C} = 0.6$ nm, with $d = 5$ nm and $N = 100$, was evaluated up to a temperature of 300°C. Using the wafer-curvature measurement system described above, we monitored stress in this film as it was heated to 100°C at a rate of 5°C/min, held at 100°C for 30 min, and then allowed to cool to room temperature. We measured both EUV and x-ray reflectance of this film before and after thermal cycling. The process was then repeated for heating to 200°C, and then to 300°C. The results are shown in Fig. 10.

The as-deposited stress in the film was measured to be -481 MPa. From the stress-temperature data [Fig. 10(a)], we see a linear change in stress as the sample is heated to 100°C, and also upon cooling back to room temperature. A linear variation of stress with temperature is expected due to the mismatch in thermal expansion coefficient between the film and the substrate. However, we see a steady drop in compressive film stress as the sample is held at 100°C, and after cooling the stress has fallen to -407 MPa. This irreversible change in stress after thermal cycling to 100°C could be due to a number of causes relating to changes in the layer microstructure and interface properties of the film [20]. But in spite of this irreversible stress change, and regardless of its cause, the EUV data [Fig. 10(b)] indicate only a slight reduction in peak EUV reflectance after cycling to 100°C, from $R_{\max} = 0.42$ to

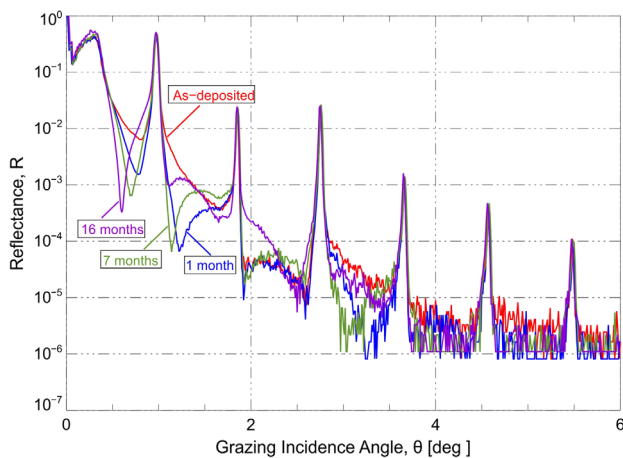


Fig. 9. XRR measurements of a Pd/B₄C/Y multilayer having barrier layers of thickness $d_{B_4C} = 0.7$ nm, made periodically over 16 months, as indicated.

$R_{\max} = 0.41$; the XRR data [Fig. 10(c)] reveal no large structural changes. Upon cycling to 200°C, the film begins to show irreversible stress relaxation at around 120°C, more relaxation as the sample is held at 200°C, and then a linear decrease in stress as the sample is cooled to room temperature. The stress after 200°C cycling has dropped to -75 MPa. While the peak EUV reflectance remains at $R_{\max} = 0.41$, there is a slight shift

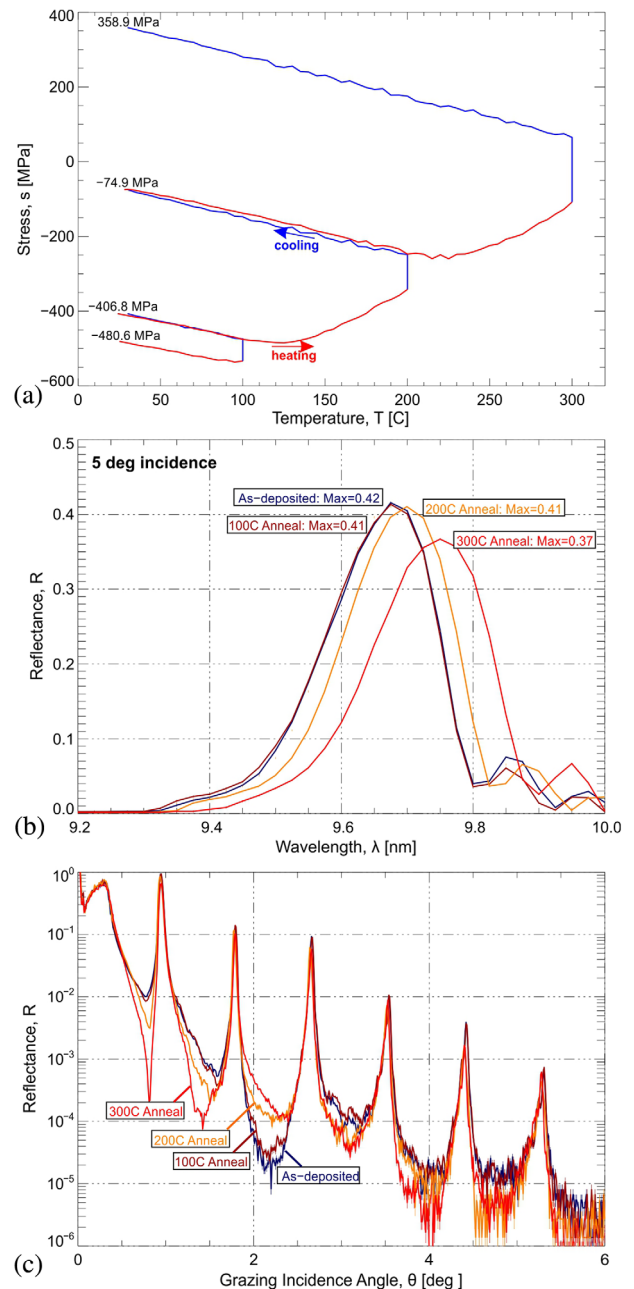


Fig. 10. (a) Stress-temperature curves for a Pd/B₄C/Y multilayer having $d_{B_4C} = 0.6$ nm, $d = 5.0$ nm, and $N = 100$. The film was heated to 100°C at a rate of 5°C/min, held at 100°C for 30 min, and then allowed to cool to room temperature. The process was repeated for thermal cycling to 200°C and 300°C, as shown. (b) EUV reflectance measurements of the film shown in (a), after cycling to 100°C, 200°C, and 300°C, as indicated. (c) XRR measurements of the same film after thermal cycling.

in the reflectance peak toward longer wavelengths; small changes in XRR are visible as well, including changes in reflectance in the range of angles between Bragg peaks, and a slight shift toward a larger multilayer period that is consistent with the observed shift in EUV reflectance. During thermal cycling to 300°C, we again see a linear change in stress up to about 200°C, then a large irreversible change in stress as the film is heated further to 300°C. The stress continues to change as the sample is held at 300°C, and then the stress falls linearly as the sample is cooled back to room temperature. The final stress is +359 MPa (tensile). After heating to 300°C, there is a significant reduction in peak EUV reflectance, to $R_{\max} = 0.37$, and a shift of ~ 0.1 nm toward longer wavelengths in the position of the multilayer peak; the XRR data indicate a corresponding increase in period after heating to 300°C, along with a reduction in the height of the first-order Bragg peak, and additional changes in reflectance between Bragg peaks.

G. HRTEM Analysis of Pd/B₄C and Pd/B₄C/Y

High-resolution transmission electron microscopy (HRTEM) analysis was performed by Evans Analytical Group (Sunnyvale, CA) on two periodic multilayers, one containing eight repetitions of Pd/B₄C, the other containing 10 repetitions of Pd/B₄C/Y/B₄C with $d_{\text{B}_4\text{C}} = 0.6$ nm. Both films have a period $d \sim 5$ nm. Cross-sectional samples were prepared using the *in situ* focused ion-beam (FIB) lift-out technique with an FEI 835 Dual Beam FIB/SEM. Samples were imaged using an FEI Tecnai TF-20 transmission electron microscope operated at 200 kV in bright-field mode. The results are shown in Fig. 11, where we compare the bottom six repetitions of each film at the highest magnification. Selected area electron diffraction (SAED) patterns are included as inserts. Both films show relatively smooth, well-defined layers. Lattice fringes are visible in the Pd layers in the Pd/B₄C multilayer, and the SAED image for this sample shows a diffraction pattern with sixfold symmetry, indicating that the Pd layers in this film are polycrystalline. There is no evidence of crystallinity in either the Pd or Y layers in the Pd/B₄C/Y film, however. The Pd/B₄C/Y film also shows somewhat smoother, sharper interfaces, consistent with the higher EUV reflectance found in this type of structure.

4. SUMMARY AND CONCLUSIONS

We have investigated the performance of periodic multilayers comprising repetitions of Pd/Y and Ru/Y, both with and without B₄C barrier layers, as well as Pd/B₄C multilayers deposited using reactive sputtering with an Ar:N₂ mixture in order to reduce film stress. Pd/Y multilayers with B₄C barrier layers were found to work well, while the other material combinations were all found to have relatively poor EUV performance. We have demonstrated that periodic Pd/Y multilayer coatings with 0.6-nm-thick B₄C barrier layers at each interface provide higher reflectance than both Pd/B₄C and Mo/Y multilayers, and do not suffer from the exceedingly high stress found in Pd/B₄C films. As a result of its higher peak reflectance, as exemplified in Fig. 6, a two-reflection telescope using Pd/B₄C/Y multilayers in place of Mo/Y multilayers tuned to the solar coronal Fe XVIII line near 9.4 nm would result in an increase in effective area by a factor of $(0.43/0.33)^2 = 1.7$.

We have also compared the EUV reflectance of Mo/Y, Pd/B₄C, and Pd/B₄C/Y coatings designed for broad spectral response near 10 nm, including dual-stack coatings tuned to 9.4 nm and 13.1 nm wavelength, and nonperiodic multilayers designed for the 8.9–11.2 nm band: while none of the nonperiodic coatings had a reflectance curve that matched the design curve with high accuracy, likely due to layer thickness errors, the growth of surface oxides, and/or inaccurate optical constants, broadband Pd/B₄C/Y multilayers nevertheless provide higher reflectance than either Mo/Y and Pd/B₄C films having similar designs, with significantly lower stress than Pd/B₄C. Broadband films such as those described here could be used for high-resolution spectroscopy instruments using multilayer-coated gratings, provided that the reflectance is judged to be sufficiently high for the application.

Periodic Pd/B₄C/Y multilayers have been shown to have reasonably good temporal stability, with a measured drop in peak reflectance from $R_{\max} = 0.38$ to $R_{\max} = 0.34$ over a period of 16 months. XRR measurements suggest either the growth over time of a surface oxide at the top-most Pd layer, small structural or chemical changes at the interfaces, or both. Future temporal stability investigations are needed to address this question definitively. Pd/B₄C/Y multilayers show no

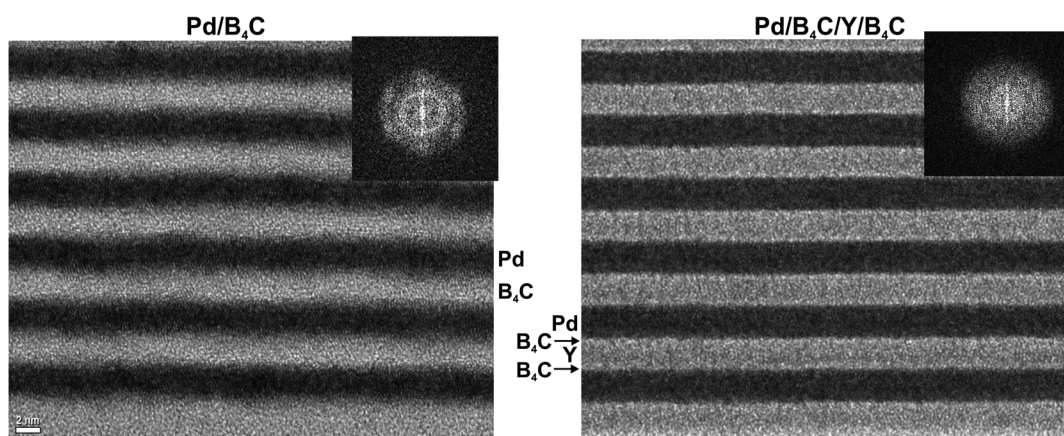


Fig. 11. HRTEM analysis of multilayers containing repetitions of either Pd/B₄C (left) or Pd/B₄C/Y/B₄C with $d_{\text{B}_4\text{C}} = 0.6$ nm (right), with a period of $d \sim 5$ nm in both cases. SAED patterns from each film are shown as insets in the upper-right corner in each case.

significant change in EUV reflectance upon thermal annealing to 100°C; heating to higher temperatures results in a slight reduction in peak reflectance and a slight shift toward longer wavelengths, indicative of an increase in multilayer period.

HRTEM analysis indicates that Pd/B₄C/Y multilayers are fully amorphous, and have smoother interfaces than similar Pd/B₄C films, which have polycrystalline Pd layers. While the reason for the difference in Pd crystallinity between the two films is unclear, the amorphous Pd layers observed in Pd/B₄C/Y multilayers may be responsible for the smoother interfaces observed in that structure.

It may be possible to further improve the performance and stability of Pd/B₄C/Y coatings through a more comprehensive investigation of B₄C barrier layer thickness—e.g., using different barrier layer thicknesses at the Pd-on-Y and the Y-on-Pd interfaces—and by designing capping layer structures that are insensitive to oxide growth, as has been done for other multilayer films [3]. Other barrier layer materials, such as C, Cr, Mo, or W, might provide better performance as well. Improvements in deposition rate calibrations for Pd, Y, and B₄C, as well as the use of a deposition system having better run-to-run stability than the system used here, would help in the realization of aperiodic multilayer coatings that more closely match the design response. Furthermore, while optical constants for B₄C have been recently measured in the wavelength range of interest here [21], more accurate optical constants for Pd and Y would also help in the development of more accurately realized nonperiodic coatings.

NASA (NNG14PN04P, NNX13CM20P, NNX14AH64G).

D. Windt gratefully acknowledges many useful discussions with A. Daw and D. Rabin of NASA GSFC, whose crucial guidance and support has helped advance the research described here.

REFERENCES AND NOTES

1. D. G. Stearns, R. S. Rosen, and S. P. Vernon, "Fabrication of high-reflectance Mo-Si multilayer mirrors by planar-magnetron sputtering," *J. Vac. Sci. Technol. A* **9**, 2662–2669 (1991).
2. C. Montcalm, P. A. Kearney, J. M. Slaughter, B. T. Sullivan, M. Chaker, H. Pépin, and C. M. Falco, "Survey of Ti-, B-, and Y-based soft x-ray-extreme ultraviolet multilayer mirrors for the 2- to 12-nm wavelength region," *Appl. Opt.* **35**, 5134–5147 (1996).
3. A. J. Corso, P. Zuppella, D. L. Windt, M. Zangrando, and M. G. Pelizzo, "Extreme ultraviolet multilayer for the FERMI@Elettra free electron laser beam transport system," *Opt. Express* **20**, 8006–8014 (2012).
4. C. Montcalm, B. T. Sullivan, M. Ranger, J. M. Slaughter, P. A. Kearney, C. M. Falco, and M. Chaker, "Mo/Y multilayer mirrors for the 8–12 nm wavelength region," *Opt. Lett.* **19**, 1173–1175 (1994).
5. B. Sae-Lao and C. Montcal, "Molybdenum-strontium multilayer mirrors for the 8–12 nm extreme-ultraviolet wavelength region," *Opt. Lett.* **26**, 468–470 (2001).
6. B. Kjomrattanawanich and S. Bajt, "Structural characterization and lifetime stability of Mo/Y extreme-ultraviolet multilayer mirrors," *Appl. Opt.* **43**, 5955–5962 (2004).
7. S. O. Kastner, W. M. Neupert, and M. Swartz, "Solar-flare emission lines in the range from 66 to 171 Å; 2s'2p^k-2s^r1'2p^{k+1} transitions in highly ionized iron," *Astrophys. J.* **191**, 261–270 (1974).
8. J. R. Lemen, A. M. Title, D. J. Akin, P. F. Boerner, C. Chou, J. F. Drake, D. W. Duncan, C. G. Edwards, F. M. Friedlaender, G. F. Heyman, N. E. Hurlburt, N. L. Katz, G. D. Kushner, M. Levay, R. W. Lindgren, D. P. Mathur, E. L. McFeaters, S. Mitchell, R. A. Rehse, C. J. Schrijver, L. A. Springer, R. A. Stern, T. D. Tarbell, J.-P. Wuelser, C. J. Wolfson, C. Yanari, J. A. Bookbinder, P. M. Cheimets, D. Caldwell, E. E. Deluca, R. Gates, L. Golub, S. Park, W. A. Podgorski, R. I. Bush, P. H. Scherrer, M. A. Gummin, P. Smith, G. Auken, P. Jerram, P. Pool, R. Soufli, D. L. Windt, S. Beardsley, M. Clapp, J. Lang, and N. Waltham, "The atmospheric imaging assembly (AIA) on the Solar Dynamics Observatory (SDO)," *Solar Phys.* **275**, 17–40 (2012).
9. D. Martínez-Galarce, R. Soufli, D. L. Windt, M. Bruner, E. Gullikson, S. Khatri, E. Spiller, J. C. Robinson, S. Baker, and E. Prast, "Multisegmented, multilayer-coated mirrors for the Solar Ultraviolet Imager," *Opt. Eng.* **52**, 095102 (2013).
10. K. Kobayashi, J. Cirtain, A. R. Winebarger, K. Korreck, L. Golub, R. W. Walsh, B. De Pontieu, C. DeForest, A. Title, S. Kuzin, S. Savage, D. Beabout, B. Beabout, W. Podgorski, D. Caldwell, K. McCracken, M. Ordway, H. Begner, R. Gates, S. McKillop, P. Cheimets, S. Platt, N. Mitchell, and D. Windt, "Hi-C: the high resolution coronal imager," *Solar Phys.* **289**, 4393–4412 (2014).
11. A. N. Daw, J. Brosius, E. Criscuolo, J. Davila, J. P. Haas, G. Hilton, D. Linard, T. Plummer, D. Rabin, R. Thomas, D. Varney, and T. Wang, "New capabilities of the EUNIS sounding rocket instrument," *Bull. Am. Astron. Soc.* **43**, (2011).
12. D. G. Stearns, R. S. Rosen, and S. P. Vernon, "Normal incidence x-ray mirror for 7 nm," *Opt. Lett.* **16**, 1283–1285 (1991).
13. D. L. Windt, "Reduction of stress and roughness by reactive sputtering in W/B₄C multilayer films," *Proc. SPIE* **6688**, 66880R (2007).
14. J. A. Bellotti and D. L. Windt, "Depth-graded Co/C multilayers prepared by reactive sputtering," *Proc. SPIE* **7437**, 743715 (2009).
15. D. L. Windt, "IMD—Software for modeling the optical properties of multilayer films," *Comput. Phys.* **12**, 360–370 (1998).
16. D. L. Windt and W. K. Waskiewicz, "Multilayer facilities for EUV lithography," *J. Vac. Sci. Technol. B* **12**, 3826–3832 (1994).
17. E. M. Gullikson, S. Mrowka, and B. B. Kaufmann, "Recent developments in EUV reflectometry at the advanced light source," *Proc. SPIE* **4343**, 363–373 (2001).
18. The algorithms used in the design of aperiodic multilayers in IMD version 5 are described in detail in the on-line documentation, available at <http://www.rxollc.com/imd>.
19. J. Gautier, F. Delmotte, M. F. Ravet, A. Jérôme, F. Bridou, F. Vernière, and F. Auchère, "Two channel multilayer mirrors for astrophysics," *Opt. Commun.* **281**, 3032–3035 (2008).
20. R. R. Kola, D. L. Windt, W. K. Waskiewicz, B. E. Weir, R. Hull, G. K. Celler, and C. A. Volkert, "Stress relaxation in Mo/Si X-ray multilayer structures," *Appl. Phys. Lett.* **60**, 3120–3122 (1992).
21. R. Soufli, A. L. Aquila, F. Salmassi, M. Fernández-Perea, and E. M. Gullikson, "Optical constants of magnetron-sputtered boron carbide thin films from photoabsorption data in the range 30 to 770 eV," *Appl. Opt.* **47**, 4633–4639 (2008).